Shear viscosity of molten alkali halides from equilibrium and nonequilibrium molecular-dynamics simulations

N. Galamba and C. A. Nieto de Castro
Departamento de Química e Bioquímica e Centro de Ciências Moleculares e Materiais, Faculdade de Ciências da Universidade de Lisboa, 1749-016 Lisboa, Portugal

James F. Ely[a)]
Chemical Engineering Department, Colorado School of Mines, Golden, Colorado 80401-1887

(Received 14 January 2005; accepted 6 April 2005; published online 10 June 2005)

The shear viscosity of molten NaCl and KCl was calculated through equilibrium (EMD) and nonequilibrium molecular-dynamics (NEMD) simulations in the canonical (N,V,T) ensemble. Two rigid-ion potentials were investigated, namely, the Born–Mayer–Huggins–Tosi–Fumi potential and the Michielsen–Woerlee–Graaf–Ketelaar potential with the parameters proposed by Ladd. The NEMD simulations were performed using the SLLOD equations of motion [D. J. Evans and G. P. Morriss, Phys. Rev. A **30**, 1528 (1984)] with a Gaussian isokinetic thermostat and the results are compared with those obtained from Green–Kubo EMD (N,V,T) simulations and experimental shear viscosity data. The NEMD zero strain rate shear viscosity, $\eta(0)$, was obtained by fitting a simplified Carreau-type equation and by application of mode-coupling theory, i.e., a η-$\gamma^{1/2}$ linear relationship. The values obtained from the first method are found to be significantly lower than those predicted by the second. The agreement between the EMD and NEMD results with experimental data is satisfactory for the two potentials investigated. The ion-ion radial distribution functions obtained with the two rigid-ion potentials for both molten salts are discussed in terms of the differences between the two models. © *2005 American Institute of Physics*.
[DOI: 10.1063/1.1924706]

I. INTRODUCTION

Difficulties related to high-temperature molten salt experiments have long motivated the use of theoretical and simulation approaches to access their properties. The experimental data available for properties such as the shear viscosity and thermal conductivity of these materials are especially scarce even though these are of both scientific and industrial interest. The latter relates to the use of molten carbonates (Na_2CO_3, K_2CO_3, and Li_2CO_3) as electrolytes in high-temperature fuel cells, which is of special interest to the authors. Furthermore, even though simple molten salts have been the subject of simulation studies for many years, the number of simulations reported for the thermal transport coefficients of these materials is very small as compared to those reported for simple nonionic fluids.

Recently, the authors investigated the shear viscosity[1] and thermal conductivity[2] of molten NaCl and KCl at different thermodynamic state points using Green–Kubo equilibrium molecular-dynamics (EMD) simulations in the microcanonical (N,V,E) ensemble. The results of those simulations showed that the Born–Mayer–Huggins–Tosi–Fumi[3–8] (BMHTF) interionic potential overpredicts the two transport coefficients generally to within 10%–15% for the shear viscosity and 10%–20% for the thermal conductivity.

Molten alkali halides are relatively simple systems being composed by univalent monatomic ions, and occupy, in the simulation of ionic liquids, the place of rare gases in the simulation of nonionic liquids. Most of the molecular simulations reported in literature for molten alkali halides use the BMHTF interionic potential.[9–16] Generally, a reasonable description of the thermodynamics, microscopic structure, and transport coefficients is found with this potential in spite of its neglect of ion-induced dipole (polarization) interactions. These effects can be taken into account in molecular-dynamics simulations through the use of shell-model potentials, several of which have been investigated in the study of both solid and fused salts.[17–21] Even though shell-model potentials are more rigorous, they significantly increase the time of computation and the differences in the simulated properties are not always significant as compared to those obtained from rigid-ion potentials.[20,21] We also note that the accuracy of the BMHTF rigid-ion potential is not equal for all the alkali halides. The omission of polarization effects, especially for large ions, is believed to play a decisive role in these discrepancies but other reasons have been pointed to in the past.[22]

With the goal of correcting for part of these deficiencies Michielsen *et al.*[23] proposed a different form for the repulsion term and derived a new set of potential parameters from solid-state data for the 17 alkali halides that have the crystal structure of NaCl. The authors discussed the possibility of this new repulsion term partially taking into account the polarization effects omitted in rigid-ion potentials. Further, the parameters proposed by Ladd[24] for the van der Waals inter-

[a)]Author to whom correspondence should be addressed. Fax: 303-273-3730. Electronic mail: jely@mines.edu

actions were used instead of the values developed by Mayer[5] for the BMHTF potential. The use of Ladd's parameters and the proposed modification of the repulsion term were based on the lattice dynamics and cell model studies[22] that suggested that the repulsion for alkali halides should be harder and the dispersion energy should be larger than those of the BMHTF potential. This potential is referred to hereinafter as the Michielsen–Woerlee–Graaf–Ketelaar–Ladd (MWGKL) potential.

The repulsion term in the MWGKL potential is significantly harder than that of the BMHTF potential. We note that a different effective pair potential had been previously proposed by Woodcock[25] based on spectroscopic data of ion pairs in the gas phase. Woodcock also found a repulsion term harder than that of the BMHTF potential. The potentials proposed by Michielsen *et al.* are harder than the BMHTF potentials but softer than those obtained by Woodcock. The dispersion energies predicted by Ladd's parameters are also larger than those obtained by Mayer. Furthermore the relation between the magnitudes of the dipole-dipole and dipole-quadrupole dispersion energies for the three types of interactions, $++$, $+-$, and $--$, predicted by Ladd's parameters, is not consistent with those of Mayer. Ladd's parameters were calculated using polarizabilities based on the static dielectric constant, which are significantly larger than those based on the high-frequency dielectric constant. Sangster and Dixon[26] discussed the lack of physical meaning in Ladd's approach, pointing out that the origin of the van der Waals interactions lies in a second-order coupling to higher electronic states which invalidates the use of the polarizabilities related to the static dielectric constant. However, the repulsion term proposed by Michielsen *et al.* implies, in terms of a rigid-ion potential, a dispersion energy larger than that predicted by the parameters of Mayer. Hence, even though Ladd's parameters may be in error they have to be used to balance the harder repulsion of the MWGKL potential. We also note that other sets of parameters for the van der Waals dispersion forces have been proposed in the past.[26] Here, however, we limit our study to the BMHTF and the MWGKL potentials with their original parameters for the specific cases of NaCl and KCl.

In this work we investigate the temperature dependence of the shear viscosity of molten NaCl and KCl through nonequilibrium molecular-dynamics (NEMD) simulations in the canonical ensemble using two rigid-ion potentials and compare it with that obtained through Green–Kubo EMD (N,V,T) simulations. The objective of this study is twofold: (1) to study the effect of a harder repulsion and stronger van der Waals interactions in the shear viscosity of molten alkali halides and (2) to investigate the accuracy with which the equilibrium (zero shear) shear viscosity of molten alkali halides can be computed through NEMD simulations. The shear viscosity is an appropriate property for this purpose because of its strong dependence on the short-range interionic forces. We have also calculated the ion-ion radial distribution functions at a single state point near their melting points using the two rigid-ion potentials for both molten NaCl and KCl.

The shear viscosity is calculated through EMD and NEMD simulations. The SLLOD equations of motion[27,28] with a Gaussian thermostat were used in conjunction with the Lees–Edwards[29] periodic boundary conditions. The Ewald sum was used to calculate the Coulombic forces and potential energy with the modification proposed by Wheeler *et al.*[30] for NEMD simulations of the shear viscosity using the Lees–Edwards boundary conditions. We also compare two methods to obtain the zero strain rate (Newtonian) viscosity from NEMD simulation data. In particular, we have obtained $\eta(0)$ from an application of Carreau's model[31,32] and by utilizing mode-coupling theory predictions.

This paper is organized as follows: Sec. II presents a description of the EMD and NEMD methods for the calculation of the shear viscosity using, respectively, the Green–Kubo approach and the SLLOD equations of motion. The two rigid-ion potential models together with the simulations parameters used in this work are discussed in Sec. III. The results of this study are discussed in Sec. IV and the conclusions are presented in Sec. V.

II. SIMULATION METHODS

A. Green–Kubo EMD simulations

The shear viscosity can be calculated from EMD simulations through integration of the stress autocorrelation function. The Green–Kubo formula for the shear viscosity is given by[33]

$$\eta = \frac{1}{3VkT}\int_0^\infty \left\langle \sum_{xy} J_{xy}(t)J_{xy}(0)\right\rangle dt, \tag{1}$$

where the stress tensor element, J_{xy}, is

$$J_{xy} = \sum_i^N P_{ix}P_{iy}/m_i + \sum_i^{N-1}\sum_{j>i}^{N} y_{ij}F_{ijx}, \tag{2}$$

and the time average in Eq. (1) involves the sum over the three different off-diagonal elements of the stress tensor, $J_{\alpha\beta}=J_{\beta\alpha}$. For a Coulombic system for which the Ewald method is used, Eq. (2) is only used for the real-space part of the force. For the reciprocal space part of the stress tensor's potential term, the product $y_{ij}F_{ijx}$ must be calculated as a whole in the Fourier space because the Fourier forces are not pairwise additive.[34,35] For monatomic ionic systems the stress tensor elements can be calculated by[35]

$$\begin{aligned} J_{xy} = {} & \sum_i^N m_i v_{ix}v_{iy} + \sum_l^{N-1}\sum_{j>1}^{N} r_{ij,x}F^R_{ij,y} \\ & + \frac{1}{2\pi L}\sum_{\mathbf{h}\neq 0} A(\mathbf{h})B_{xy}\left[\sum_{i=1}^N Z_i \cos\left(\frac{2\pi}{L}\mathbf{h}\cdot\mathbf{r}_i\right)\right]^2 \\ & + \left[\sum_{i=1}^N Z \sin\left(\frac{2\pi}{L}\mathbf{h}\cdot\mathbf{r}_i\right)\right]^2, \end{aligned} \tag{3}$$

where

$$A(\mathbf{h}) = \frac{\exp\left(-\frac{\pi^2|\mathbf{h}|^2}{\alpha^2 L^2}\right)}{|\mathbf{h}|^2}, \tag{4}$$

and for the xy component of the tensor $\mathbf{B}(\mathbf{h})$,

$$B_{xy} = \delta_{xy} - \frac{2|\mathbf{h}_x||\mathbf{h}_y|}{|\mathbf{h}|^2} - \left(\frac{2\pi}{L}\right)^2 \frac{|\mathbf{h}_x||\mathbf{h}_y|}{2\alpha^2}. \tag{5}$$

In Eq. (3) F^R includes the short-range forces and the real part of the Ewald–Coulomb forces, both computed in the real space.

B. NEMD simulations

For a system undergoing planar Couette flow with strain rate, $\gamma = \partial u_x / \partial y$, the thermostatted SLLOD equations of motion are given by[27,28]

$$\dot{\mathbf{r}}_i = \frac{\mathbf{p}_i}{m_i} + \mathbf{i}\gamma y_i, \quad \dot{\mathbf{p}}_i = \mathbf{F}_i - \mathbf{i}\gamma P_{y,i} - \zeta \mathbf{p}_i, \tag{6}$$

where $\dot{\mathbf{r}}_i$ is the velocity and $\mathbf{p}_i$ the linear momentum of particle i, $\mathbf{F}_i$ is the force on particle i resulting from the interaction with all the particles of the system, $\mathbf{i}$ is the x-unit vector, and ζ is the Gaussian thermostat[28] multiplier given by

$$\zeta = \frac{\sum_{i=1}^{N} (\mathbf{F}_i \cdot \mathbf{p}_i - \gamma p_{xi} p_{yi})/m_i}{\sum_{i-1}^{N} (\mathbf{p}_i \cdot \mathbf{p}_j)/m_i}. \tag{7}$$

The shear viscosity can be calculated from the J_{xy} element of the stress tensor using the following relation:

$$\eta = -\frac{\langle J_{xy} \rangle}{\gamma V}, \tag{8}$$

where V is the volume, J_{xy} is given by Eq. (3), and the brackets indicate a steady-state average value.

The Lees–Edwards "sliding-brick" boundary conditions[29] were used with Wheeler's[30] modification for the reciprocal space lattice. This modification ensures that the calculation of the interaction between particle i and j and all of its images in the reciprocal space lattice of the Ewald sum accounts for the same amount of shear offset that is imposed on the particles' interactions in the real-space lattice (using the minimum image convention and spherical truncation) by the Lees–Edwards boundary conditions. The NEMD method with the use of Lees–Edwards boundary conditions requires the use of a sheared lattice from which the positions of the particles in the normal cubic reciprocal space lattice are reassigned to occupy the positions on a lattice no longer composed of cubic cells.[30] Thus geometrically this transformation reassigns the particles' positions from a cubic cell ($L_1 = L_2 = L_3 = L$ and $\theta_{12} = \theta_{13} = \theta_{23} = \pi/2$) to a parallelepiped simulation cell [$L_1 = L_3 = L, L_{2'} = L_2(1+\chi^2)^{1/2}$ and $\theta_{13} = \theta_{2'3} = \pi/2, \theta_{12'} = \pi/2$-arcsin $[\chi/(1+\chi^2)^{1/2}]$], where L_k is the length of the k side of the box and $\chi = \gamma t$ is the strain ($\gamma = \partial u_x / \partial y$ is the constant shear rate at which the simulation is performed and t the elapsed time). During a simulation $L_{2'}$ and $\theta_{12'}$, oscillate, respectively, between $L_2 \leqslant L_{2'} \leqslant L_2\sqrt{2}$ and $\pi/4 \leqslant \theta_{12'} \leqslant \pi/2$, which corresponds to $0 \leqslant \chi \leqslant 1$. This interval for the strain was used here for both the real- and reciprocal space calculations. Hence, using this method, the reciprocal space part of the Ewald–Coulomb force on particle i (e.g., x component) is calculated by

$$F_{x,i} = \frac{2Z_i}{L^2} \sum_{\mathbf{h}} A(\mathbf{h}) h_x \left\{ \sin\left(\frac{2\pi}{L}\mathbf{h} \cdot \mathbf{r}_i\right) \sum_{j-1}^{N} Z_j \cos\left(\frac{2\pi}{L}\mathbf{h} \cdot \mathbf{r}_j\right) - \cos\left(\frac{2\pi}{L}\mathbf{h} \cdot \mathbf{r}_i\right) \sum_{j=1}^{N} Z_j \sin\left(\frac{2\pi}{L}\mathbf{h} \cdot \mathbf{r}_j\right) \right\}, \tag{9}$$

with the internal product $\mathbf{h} \cdot \mathbf{r}_i$ (and $\mathbf{h} \cdot \mathbf{r}_j$) given by

$$\mathbf{h} \cdot \mathbf{r}_i = [h_x(x_i - \chi y_i) + h_y y_i + h_z z_i], \tag{10}$$

where the particle coordinates are the same as those used in the real-space calculations. Further, Eq. (10) is used in the calculation of the stress tensor elements given by Eq. (3). This transformation is simply a consequence of the equivalence between Lees–Edwards sliding-brick and deforming box periodic boundary conditions; alternatively one can use deforming box boundary conditions for both the real- and reciprocal space lattices.[36]

III. INTERIONIC POTENTIALS AND SIMULATION PARAMETERS

The BMHTF interionic potential has the following form:

$$u_{ij}(r) = \frac{Z_i Z_j e^2}{r} + A_{ij} \exp\left[B(\sigma_{ij} - r)\right] - \frac{C_{ij}}{r^6} - \frac{D_{ij}}{r^8}, \tag{11}$$

where the first term is the Coulomb interaction, the second the Born–Huggins exponential repulsion, and the third and fourth terms correspond to the dipole-dipole and dipole-quadrupole dispersion energies. The MWGKL pair potential is given by

$$u_{ij}(r) = \frac{Z_i Z_j e^2}{r} + \frac{b}{r^n} \exp\left[k_{ij}(\sigma_{ij}^m - r^m)\right] - \frac{C_{ij}}{r^6} - \frac{D_{ij}}{r^8}, \tag{12}$$

where the parameters b and k are common for the three interactions for every molten salt and are given by the authors for the 17 alkali halides with the structure of sodium chloride. The values of b and k were given for $m = 1$ and $n = 0$, 4, 5, and 6. Following Michielsen *et al.* (1975) we investigate the potential with $m = 1$ and $n = 4$ that was used in their simulations.

In spite of the differences between the two potentials in the repulsion and the van der Waals dispersion energy, the minimum of the potentials for the cation-anion interactions in NaCl and KCl are not very different. The inter-ion separation distance at the minimum is smaller for the BMHTF potential but the energy depth is similar for the two potentials. Comparing the like ion interactions, the overall MWGKL potential is harder than the BMHTF potential for the (Na^+, Na^+) pair but not for (Cl^-, Cl^-) in NaCl. For the case of KCl the MWGKL potential is harder for (Cl^-, Cl^-) but not for the (K^+, K^+) pair.

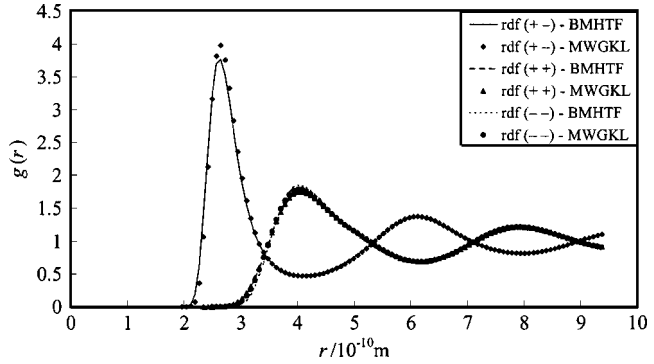

FIG. 1. Ion-ion radial distribution functions (rdf) for NaCl obtained with the BMHTF and the MWGKL interionic potentials.

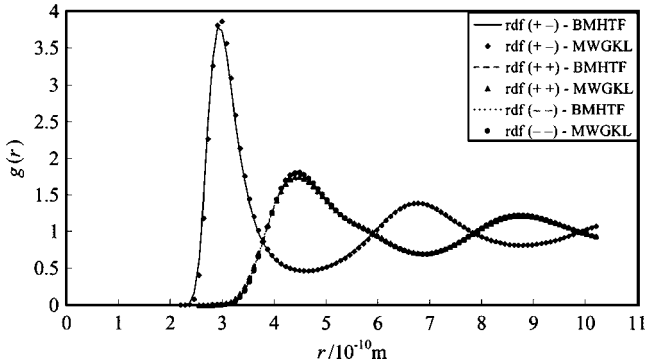

FIG. 2. Ion-ion rdf for KCl obtained with the BMHTF and the MWGKL interionic potentials.

For the simulations reported here, the value of the convergence parameter α in the Ewald sum was set equal to $5.6/L$ with a truncation of the real part of the Ewald–Coulomb potential at $r_c = L/2$ and the Fourier part of the force and potential energy was summed up to the vector $|\mathbf{h}|^2_{\max} = 27$, with the k-space vector given by $\mathbf{k} = 2\pi\mathbf{h}/L$. The simulations have been performed in the canonical ensemble for a cubic sample composed of $N = 216$ ions using periodic boundary conditions (pbc) and the minimum image convention. The positions at time zero were defined as those corresponding to the face-centered-cubic lattice of solid NaCl and the zero time velocities were defined randomly and scaled to ensure a zero total linear momentum. A fifth-order Gear algorithm for first-order differential equations was used to solve the equations of motion[37] with a time step of 1.0 fs. The NEMD shear viscosity, $\eta(\gamma)$, was calculated from simple block averages of 10 000 time steps each from 1.5×10^6 time step (1.5 ns) production runs after 1.5×10^5 time step (0.15 ns) runs. The stress autocorrelation functions used to obtain the Green–Kubo EMD shear viscosity were calculated from 3.5×10^6 time steps (3.5 ns) production runs for most of the state points after 1.5×10^5 time steps (0.15 ns) equilibration runs.

The shear viscosity was calculated at five different temperatures, the volume at each temperature being calculated from experimental liquid density data correlations.[38] For the case of the MWGKL potential model of NaCl and KCl, NEMD simulations were performed at a single state point but Green–Kubo EMD simulations were performed for the five different state points to allow the study of the temperature dependence of the shear viscosity predicted by this potential. For the BMHTF potential both EMD and NEMD simulations were made for the five different state points for each of the molten salts.

IV. RESULTS AND COMPARISONS

A. Structure

Figures 1 and 2 display the three partial radial distribution functions, respectively, for NaCl and KCl obtained with the BMHTF and the MWGKL interionic potentials at the state points: $T = 1100$ K and $\rho = 1.5420$ g cm^{-3} for NaCl and $T = 1050$ K and $\rho = 1.5236$ g cm^{-3} for KCl. It can be seen that the only significant difference between the radial distribution functions is the height of the first peak for $g_{+-}(r)$ and to a lesser extent for $g_{++}(r)$ [first peak height: $g_{++}^{\mathrm{MWGKL}}(r) \cong g_{++}^{\mathrm{BMHTF}}(r)$ for NaCl and $g_{++}^{\mathrm{MWGKL}}(r) < g_{++}^{\mathrm{BMHTF}}(r)$ for KCl] and $g_{--}(r)$ [first peak height: $g_{--}^{\mathrm{MWGKL}}(r) < g_{--}^{\mathrm{BMHTF}}(r)$ for NaCl and $g_{--}^{\mathrm{MWGKL}}(r) > g_{--}^{\mathrm{BMHTF}}(r)$ for KCl]. Furthermore the difference between $g_{+-}(r)$ is more pronounced for the case of NaCl. The position (interionic distance) of the first and second coordination shells for the three partial radial distribution functions predicted by the two potentials is almost the same for the two molten salts. In general we expect a stiffer repulsion to cause the distance of (at least) the first coordination shell of the three partial radial distribution functions to increase, i.e., the average distance of the nearest neighbors (of unlike charge) and the second nearest neighbors (of like charge) to each ion to increase. On the other hand we expect stronger van der Waals forces to cause the opposite effect.

B. Shear viscosity

If the shear viscosity could be simulated for arbitrarily low and high shear rates using NEMD methods, then the complete rheology of the fluid could be studied from experimentally inaccessible to arbitrarily close to zero shear rates. The results of those simulations could then be easily compared to the zero shear rate viscosity obtained from Green–Kubo EMD simulations. However, because the signal-to-noise ratio is very small for SLLOD-NEMD simulations at low shear rates the Newtonian region (i.e., the region where the shear viscosity is shear rate independent) is difficult to identify. Hence, if we only have $\eta(\gamma)$ data at relatively high shear rates, the value of $\eta(0)$ obtained from NEMD simulations depends on the assumed relationship between the shear viscosity and the strain rate.

The crossover strain rate point below which the Newtonian regime occurs and above which shear thinning is expected to occur for simple fluids is related to the inverse of the longest relaxation time of the fluid in equilibrium (i.e., in the absence of shear). For simple monatomic fluids this is the translational relaxation time.[39] It turns out that this crossover point is at a strain rate that is too high to be accessed by experiments and already too low to be accessed by high precision NEMD simulations. Several methods have been investigated in the NEMD studies reported in literature to obtain $\eta(0)$ from $\eta(\gamma)$ NEMD data.[16,39–41] Here we consider two

TABLE I. Newtonian viscosities for the BMHTF and MWGKL models of NaCl calculated from GK-EMD and NEMD simulations. MC denotes a value calculated from Eq. (14). The experimental results are from the NIST database (see Ref. 38).

		BMHTF			MWGKL			Expt.
T (K)	ρ (g cm^{-3})	η^{Carreau} (mPa s)	η^{MC} (mPa s)	η^{GK} (mPa s)	η^{Carreau} (mPa s)	η^{MC} (mPa s)	η^{GK} (mPa s)	η (mPa s)
1100	1.5420	1.129	1.289	1.193	1.154	1.358	1.228	1.00
1200	1.4878	0.906	1.055	0.916	⋯	⋯	0.978	0.834
1300	1.4335	0.747	0.852	0.833	⋯	⋯	0.859	0.713
1400	1.3793	0.636	0.710	0.702	⋯	⋯	0.710	0.624
1500	1.3250	0.547	0.605	0.590	⋯	⋯	0.603	0.555

distinct approaches to predict $\eta(0)$: (1) linear extrapolation with respect to γ^{β} and (2) fitting with a simplified Carreau equation.[31,32] In the first method a relation of the form

$$\eta = \eta(0) - A\gamma^{\beta} \tag{13}$$

is used, typically with the value of β being 0.5 which is the value predicted from the mode-coupling theory for three-dimensional fluids in the limit of zero shear rate[42]

$$\lim_{\gamma \to 0} \eta(\gamma) = \eta(0) - A\gamma^{1/2}. \tag{14}$$

For molten alkali halides this relation was found to describe the shear viscosity for the specific case of NaCl (Ref. 16) and was also used in this study for KCl and NaCl. It turns out that if a large enough range of shear rates is simulated, the shear viscosity is better described by two distinct lines linearly related to $\gamma^{1/2}$, that intersect at a particular value of γ.[16,39,40] One cannot identify any of these lines with that predicted by mode-coupling theory which is valid in the limit of zero shear that is inaccessible by NEMD simulations. Several recent studies have been performed to try to resolve the problem of low shear rate NEMD including that of Borzsák *et al.*[39] who have studied the shear viscosity of the Weeks–Chandler–Andersen fluid using the transient time correlation function (TTCF) formalism over a wide range of shear rates. The results of the TTCF simulations allow one to calculate the shear viscosity at much lower shear rates with precision similar to that of the Green–Kubo. Consistency between the data obtained at lower strain rates from TTCF simulations and those at higher strain rates calculated from SLLOD-NEMD (Ref. 43) was observed for large systems. Furthermore they concluded that their low and high strain rate TTCF shear viscosity data plotted against the square root of the strain rate are better described by two different straight lines intersecting at approximately the same value of shear rate found by Travis *et al.*[40] There are, however, significant differences in the slopes of the two least-squares-fitted lines obtained with the TTCF formalism[39] and SLLOD-NEMD.[40] The slope of the line corresponding to lower strain rates obtained by Borzsák *et al.* is actually positive though close to zero which leads to the prediction of a lower value of the zero shear rate viscosity.

In this work we have not used the TTCF method and therefore the results given here do not allow one to make conclusions concerning mode-coupling theory predictions for the case of molten alkali halides. Thus, we assume here that if Eq. (13) describes (in a statistically significant sense) the shear viscosity for a specific strain rate region, it can be used to estimate $\eta(0)$, keeping in mind, however, that this may not be the same as that predicted by Eq. (14).

In addition to Eq. (13) a simplified Carreau equation[31,32] of the form

$$\frac{\eta}{\eta_0} = \left[1 + (\lambda\gamma)^2\right]^{(n-1)/2} \tag{15}$$

was fitted to obtain the zero shear rate viscosity, η_0. In this equation λ is a time constant. Another common approach (not used here) involves the use of an empirical equation (e.g., the four-parameter Cross equation)[16,39,40] to describe the complete set of shear viscosity data at different shear rates. Like the Carreau equation, this model also allows one to describe the complete set of data through a single curve giving a smooth transition between shear thinning and New-

TABLE II. Newtonian viscosities for the BMHTF and MWGKL models of KCl calculated from GK-EMD and NEMD simulations. MC denotes a value calculated with Eq. (14). The experimental results are from the NIST database (see Ref. 38).

		BMHTF			MWGKL			Expt.
T (K)	ρ (g cm^{-3})	η^{Carreau} (mPa s)	η^{MC} (mPa s)	η^{GK} (mPa s)	η^{Carreau} (mPa s)	η^{MC} (mPa s)	η^{GK} (mPa s)	η (mPa s)
1050	1.5236	1.170	1.36	1.156	1.213	1.29	1.177	1.086
1100	1.4945	1.029	1.20	1.084	⋯	⋯	1.058	0.954
1200	1.4362	0.806	0.941	0.838	⋯	⋯	0.927	0.759
1250	1.4070	0.730	0.847	0.811	⋯	⋯	0.784	0.687
1300	1.3779	0.683	0.774	0.687	⋯	⋯	0.708	0.555

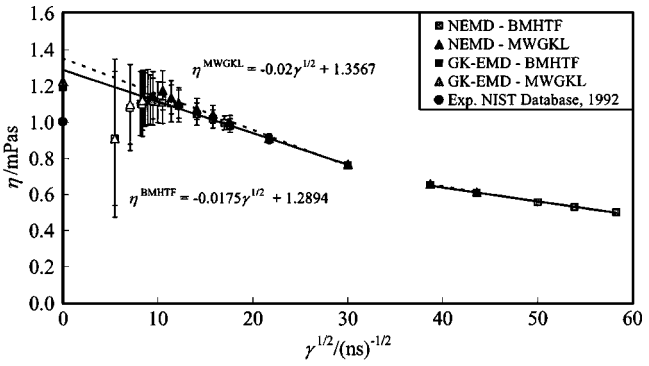

FIG. 3. NEMD shear viscosity vs the square root of the strain rate for NaCl. The data are compared with the GK-EMD shear viscosity obtained in this work and experimental data. The full and dashed lines correspond to the two least-squares fits in different strain rate regions for the BMHTF and the MWGKL potentials, respectively.

tonian rheology from which it is possible to obtain the zero shear viscosity. Tables I and II summarize the shear viscosity data obtained in this work through both Green–Kubo EMD and NEMD simulations for the BMHTF and MWGKL potential models of NaCl and KCl, respectively.

The two approaches described above for finding the Newtonian viscosity are illustrated in Figs. 3–6 for NaCl and KCl at a single state near their melting points. Figure 3 gives the shear viscosity versus the square root of the strain rate at $T=1100$ K and $\rho=1.5420$ g cm^{-3} obtained for the BMHTF and the MWGKL interionic potential models of NaCl. The standard deviation of the points at higher shear rates is lower than the size of the symbols and is not visible in Fig. 3. Figure 4 displays the Carreau analysis at the same conditions of temperature and density of Fig. 3 for the two potentials. From this plot a crossover point can be observed at a shear rate around 0.2 ps^{-1}. In both figures the NEMD data are compared with the Green–Kubo EMD (N,V,T) data obtained in this work and experimental shear viscosity. From Figs. 3 and 4 it can be seen that the two potentials predict similar (within mutual uncertainty) values for the shear viscosity, $\eta(\gamma)$, for the specific state point simulated. Figures 5 and 6 give the corresponding plots for the case of the BMHTF and the MWGKL interionic potential models of KCl at $T=1050$ K and $\rho=1.5236$ g cm^{-3}. As for the case of NaCl one can see that the shear viscosities obtained through both Green–Kubo EMD and SLLOD-NEMD are similar for the two potentials. These results indicate that the stronger repulsion and dispersion forces of the MWGKL potential have opposite but similar effects in the shear viscosity of the model fluids and therefore no significant difference is observed with relation to the BMHTF potential.

Figures 7 and 8 display the shear viscosity against the square root of the strain rate and the logarithm of the shear viscosity against the logarithm of the strain rate, respectively, at five different temperatures for the BMHTF model of NaCl. Figures 9 and 10 give the corresponding results for the case of the BMHTF model of KCl. From Figs. 7 and 9 the difficulties in using Eq. (14) to calculate $\eta(0)$ according to mode-coupling predictions are clear. The values obtained this way are therefore more correctly identified with those obtained from Eq. (13) since one cannot assure that the limit $\gamma\rightarrow 0$ coincides with the least-squares fits obtained from the NEMD shear viscosity at relatively high shear rates. We have neglected the data points at lower shear rates whenever these lead to a poor statistics of the least-squares fits. At higher temperatures (and lower densities) some of the lower strain rate shear viscosity data points fall out any statistically significant linear fit and therefore have not been taken into account in the extrapolation of $\eta(0)$. Following the discussion above, due to the large uncertainties coupled to these values of the shear viscosity and the lack of information concerning the strain rate interval for asymptotic behavior to be observed one cannot conclude that mode-coupling theory fails to describe the shear viscosity of molten alkali halides.

Figures 8(a) and 10(a) on the other hand show a relatively well-defined change in rheology and $\eta(0)$ can be easily calculated assuming that the apparent Newtonian plateau observed is that of the model fluid. It can be seen that at higher temperatures and lower densities the strain rate "size" of this Newtonian plateau increases. Hence Eq. (15) predicts a decrease of the translational relaxation time of the fluid in equilibrium at higher temperatures and lower densities. In

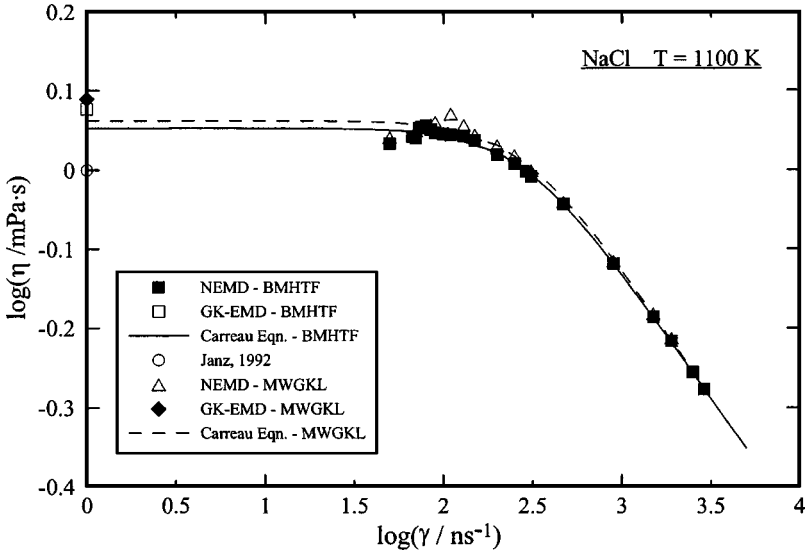

FIG. 4. Logarithm of the NEMD shear viscosity against the logarithm of strain rate for NaCl. The data are compared with the GK-EMD shear viscosity obtained in this work and experimental data. The full and dashed lines correspond to the Carreau function fits for the BMHTF and the MWGKL potentials, respectively.

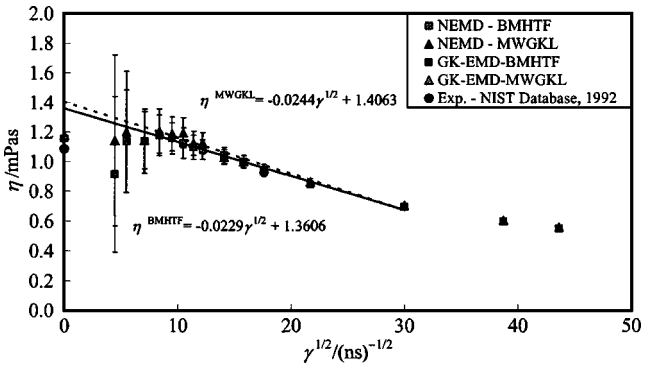

FIG. 5. NEMD shear viscosity vs the square root of the strain rate for KCl. The data are compared with the GK-EMD shear viscosity obtained in this work and experimental data. The full and dashed lines correspond to the least-squares fit for the BMHTF and the MWGKL potentials, respectively, at the lower strain region simulated.

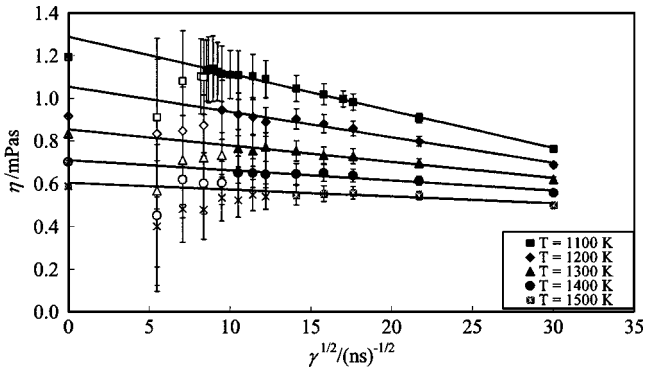

FIG. 7. NEMD shear viscosity vs the square root of the strain rate at different temperatures for the BMHTF model of NaCl. The data are compared with the GK-EMD shear viscosity obtained in this work.

Figs. 8(b) and 10(b) we have also performed temperature-time scaling[32,44] to produce master equations for the shear-dependent viscosity of NaCl and KCl. In these scalings the reference conditions were chosen to be the 1100-K simulation for NaCl and the 1050-K simulation for KCl. The scaling factors are defined by

$$a_\eta = \frac{\eta_0(T,\rho)}{\eta_0(T_{\mathrm{ref}},\rho_{\mathrm{ref}})} \text{ and } a_T = a_\eta \frac{T_{\mathrm{ref}}\rho_{\mathrm{ref}}}{T\rho}, \tag{16}$$

and scaled viscosity in terms of the Carreau equation is given by

$$\eta_s(\gamma_s) = \frac{\eta(a_T\gamma)}{a_\eta} = \eta_0(T_{\mathrm{ref}},\rho_{\mathrm{ref}})\left[1+(\lambda a_T\gamma)^2\right]^{(n-1)/2}. \tag{17}$$

In these equations the subscript "0" denotes the Newtonian viscosity and $\gamma_s = a_T\gamma$. For NaCl the parameters are $\eta_0(T_{\mathrm{ref}}\rho_{\mathrm{ref}}) = 1.126$ mPa s, $\lambda = 2.27\times10^{-12}$ s, and $n = 0.593$ while for KCl we found $\eta_0(T_{\mathrm{ref}}\rho_{\mathrm{ref}}) = 1.168$ mPa s, $\lambda = 3.82\times10^{-12}$ s, and $n = 0.641$.

Figure 11 gives an overall comparison of the shear viscosity data obtained in this work for the two potentials used

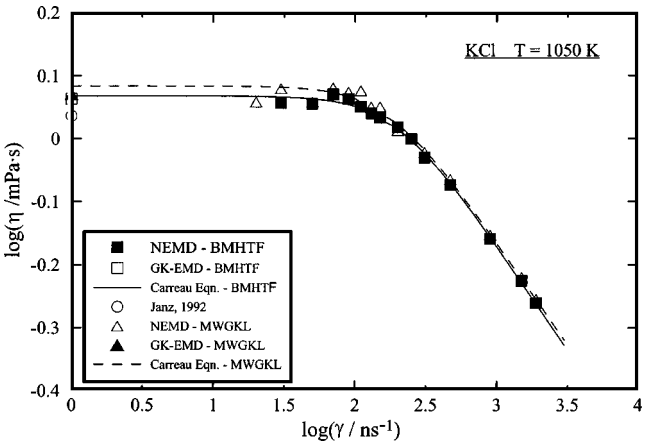

FIG. 6. Logarithm of the NEMD shear viscosity against the logarithm of strain rate for KCl. The data are compared with the GK-EMD shear viscosity obtained in this work and experimental data. The full and dashed lines correspond to the Carreau function fits for the BMHTF and the MWGKL potentials, respectively.

with experimental correlations for shear viscosity from the NIST database for molten salts.[38] The experimental correlation data for the case of sodium chloride are slightly overpredicted, the error increasing with the temperature. For the case of potassium chloride the correlation from which the viscosity has been calculated is only valid for the temperature interval of 1111–1142 K and extrapolated data have been used for the comparisons given in this work. The lower values obtained through the analysis of the NEMD simulations with Eq. (15) are in closer agreement with the experimental data. Perhaps a more relevant comparison is the deviation of the NEMD $\eta(0)$ data from the Green–Kubo EMD values. Generally these are similar ($<15\%$) for the two approaches, although of opposite sign. Hence, though relatively different, overall the values obtained from the two methods are in satisfactory agreement with that obtained from the Green–Kubo EMD method and the shear viscosity is overpredicted relative to the experimental value in both methods.

V. CONCLUSIONS

The shear viscosity of molten NaCl and KCl was computed through both equilibrium and nonequilibrium molecular-dynamics methods. Two rigid-ion potentials were investigated with the purpose of studying the combined effect of a harder repulsion and stronger dispersion forces in the shear viscosity of molten alkali halides. Further, the temperature dependence of the shear viscosity of these materials was investigated through both simulation methods for the case of the BMHTF potential and two distinct approaches were used to obtain the Newtonian (zero shear rate) viscosity from NEMD viscosity data at high shear rates. Although the zero shear rate viscosity obtained through the two methods is considerably different, a reasonable agreement was found with the Green–Kubo (GK) EMD results. The results show that the Newtonian viscosity relative to the GK results are generally underpredicted by the Carreau analysis and overpredicted by mode-coupling theory. Newtonian viscosities obtained via the Carreau equation are, however, typically in better agreement with the GK results. The shear viscosity obtained with the MWGKL potential and that calculated using the BMHTF potential was found to be in close agreement. The effects of the stronger repulsion and van der Waals forces of the MWGKL potential partially cancel out and this

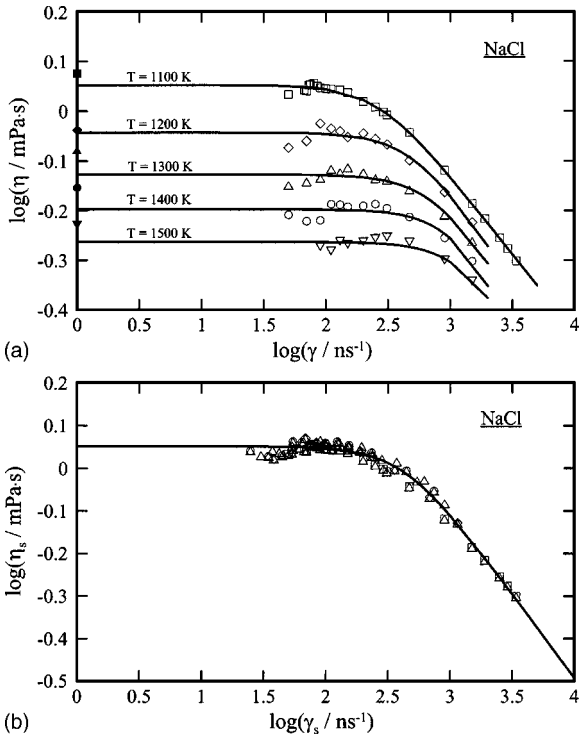

FIG. 8. (a) Logarithm of the NEMD shear viscosity against the logarithm of the strain rate at different temperatures for the BMHTF model of NaCl. The data are compared with the GK-EMD shear viscosity obtained in this work. (b) The temperature-time-scaled master equation for the shear-dependent viscosity of NaCl as given in Eq. (17).

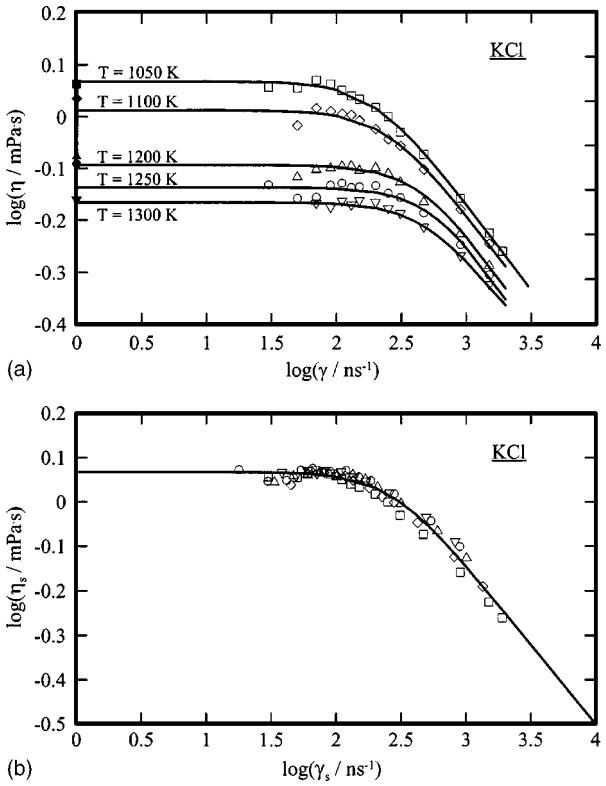

FIG. 10. (a) Logarithm of the NEMD shear viscosity against the logarithm of the strain rate at different temperatures for the BMHTF model of KCl. The data are compared with the GK-EMD shear viscosity obtained in this work. (b) The temperature-time-scaled master equation for the shear-dependent viscosity of KCl as given in Eq. (17).

fact explains the agreement between both the ion-ion radial distribution functions and the shear viscosity obtained with the two potentials.

Even though a number of problems arise in using shell-model potentials as discussed previously, we consider the extension of this study to the case of shell-model potentials for molten alkali halides to be of special interest since it may allow one to identify the weaknesses of both type of models. We also note that the effect of three-body potentials on the transport properties of molten alkali halides is unknown and should be considered in future studies as well.

Regarding the calculation methodologies for the shear viscosity, we also believe that the application of the TTCF algorithm is of special significance since it may enable one

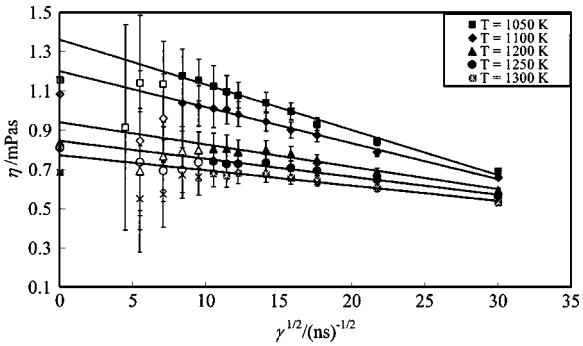

FIG. 9. NEMD shear viscosity against the square root of the strain rate at different temperatures for the BMHTF model of KCl. The data are compared with the GK-EMD shear viscosity obtained in this work.

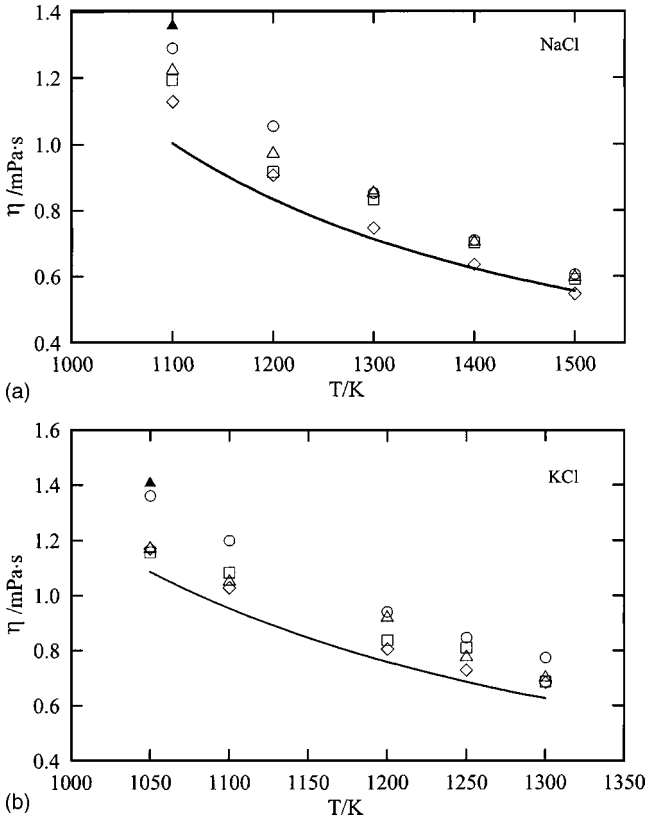

FIG. 11. Comparison between the simulation and experimental shear viscosity for (a) NaCl and (b) KCl. Solid line: Janz (Ref. 38); □ GK-EMD-BMHTF; ○ NEMD-BMHTF-MC; ◇ NEMD-BMHTF: Carreau; △ GK-EMD-MWGKL; ▲ NEMD-MWGKL-MC.

to understand to what extent the Newtonian plateau of the BMHTF model of NaCl and KCl is, in fact, that predicted by Eq. (15).

ACKNOWLEDGMENTS

One of the authors (N.G.) would like to thank the Fundação para a Ciência e Tecnologia from Portugal for a Ph.D. grant under the program PRAXIS XXI/BD/19792/99, and to Colorado School of Mines, where part of this work was developed, for the opportunity provided as a visiting student. Another author (J.F.E.) was supported by the U. S. DOE Office of Science, Grant No. DE-FG03-95ER14568.

[1] N. Galamba, C. A. N. de Castro, and J. F. Ely, J. Phys. Chem. B **108**, 3658 (2004).
[2] N. Galamba, C. A. N. de Castro, and J. F. Ely, J. Chem. Phys. **120**, 8676 (2004).
[3] M. V. Born and J. E. Mayer, Z. Phys. **75**, 1 (1932).
[4] M. L. Huggins and J. E. Mayer, J. Chem. Phys. **1**, 643 (1933).
[5] J. E. Mayer, J. Chem. Phys. **1**, 270 (1933).
[6] M. L. Huggins, J. Chem. Phys. **5**, 143 (1937).
[7] M. P. Tosi and F. G. Fumi, J. Phys. Chem. Solids **25**, 45 (1964).
[8] F. G. Fumi and M. P. Tosi, J. Phys. Chem. Solids **25**, 31 (1964).
[9] L. V. Woodcock and K. Singer, Trans. Faraday Soc. **67**, 12 (1971).
[10] F. Lantelme, P. Turq, B. Quentrec, and J. Lewis, Mol. Phys. **28**, 1537 (1974).
[11] J. W. E. Lewis and K. Singer, J. Chem. Soc., Faraday Trans. 2 **71**, 41 (1975).
[12] J. W. E. Lewis, K. Singer, and L. V. Woodcock, J. Chem. Soc., Faraday Trans. 2 **71**, 301 (1975).
[13] G. Ciccotti, G. Jacucci, and I. R. McDonald, Phys. Rev. A **13**, 426 (1976).
[14] P. Sindzingre and M. J. Gillan, J. Phys.: Condens. Matter **2**, 7033 (1990).
[15] Y. Guissani and B. Guillot, J. Chem. Phys. **101**, 490 (1994).
[16] J. Delhommelle and J. Petravic, J. Chem. Phys. **118**, 2783 (2003).
[17] M. Dixon and M. J. L. Sangster, J. Phys. C **8**, L8 (1975).
[18] M. Dixon and M. J. L. Sangster, J. Phys. C **9**, L5 (1976).
[19] G. Jacucci, I. R. McDonald, and A. Rahman, Phys. Rev. A **13**, 1581 (1976).
[20] P. J. D. Lindan and M. J. Guillan, J. Phys.: Condens. Matter **5**, 1019 (1993).
[21] G. V. Paolini, P. J. D. Lindan, and J. H. Harding, J. Chem. Phys. **106**, 3681 (1997).
[22] F. H. Ree and A. C. Holt, Phys. Rev. B **8**, 826 (1973).
[23] J. Michielsen, P. Woerlee, F. van der Graaf, and J. A. A. Ketelaar, J. Chem. Soc., Faraday Trans. 2 **71**, 1730 (1975).
[24] M. F. C. Ladd, J. Chem. Phys. **60**, 1954 (1974).
[25] L. V. Woodcock, J. Chem. Soc., Faraday Trans. 2 **70**, 1405 (1974).
[26] M. J. L. Sangster and M. Dixon, Adv. Phys. **25**, 247 (1976).
[27] D. J. Evans and G. P. Morriss, Phys. Rev. A **30**, 1528 (1984).
[28] D. J. Evans and G. P. Morriss, *Statistical Mechanics of Nonequilibrium Liquids* (Academic, London, 1990).
[29] A. W. Lees and S. F. Edwards, J. Phys. C **5**, 1921 (1970).
[30] D. R. Wheeler, N. G. Fuller, and R. L. Rowley, Mol. Phys. **92**, 55 (1997).
[31] P. J. Carreau, Ph.D. thesis, University of Wisconsin, 1968.
[32] R. B. Bird, R. C. Armstrong, and O. Hassager, *Dynamics of Polymeric Liquids*, *Fluid Mechanics* Vol. 1 (Wiley, New York, 1977).
[33] R. Zwanzig, Annu. Rev. Phys. Chem. **16**, 67 (1965).
[34] S. Nosé and M. L. Klein, Mol. Phys. **50**, 1055 (1983).
[35] D. M. Heyes, Phys. Rev. B **49**, 755 (1994).
[36] S. Balasubramanian, C. K. Mundy, and M. L. Klein, J. Chem. Phys. **105**, 11190 (1996).
[37] M. P. Allen and D. J. Tildesley, *Computer Simulations of Liquids* (Clarendon, Oxford, 1997).
[38] G. J. Janz, *NIST Properties of Molten Salts Database* (NIST SRD 27, Boulder, 1992).
[39] I. Borzsák, P. T. Cummings, and D. J. Evans, Mol. Phys. **100**, 2735 (2002).
[40] K. P. Travis, D. J. Searles, and D. J. Evans, Mol. Phys. **95**, 195 (1998).
[41] Y. Yang, T. A. Pakkanen, and R. L. Rowley, Int. J. Thermophys. **21**, 703 (2000).
[42] K. Kawasaki and J. D. Gunton, Phys. Rev. A **8**, 2048 (1973).
[43] R. Bhupathiraju, P. T. Cummings, and H. D. Cochran, Mol. Phys. **88**, 1655 (1996).
[44] S. Bair, C. McCabe, and P. T. Cummings, Phys. Rev. Lett. **88**, 058302 (2002).